Objective Estimation of the 24-h Probability of Tropical Cyclone Formation

ANDREA B. SCHUMACHER

Cooperative Institute for Research in the Atmosphere–Colorado State University, Fort Collins, Colorado

MARK DEMARIA AND JOHN A. KNAFF

NOAA/NESDIS/Center for Satellite Applications and Research, Fort Collins, Colorado

(Manuscript received 31 December 2007, in final form 28 May 2008)

ABSTRACT

A new product for estimating the 24-h probability of TC formation in individual 5° × 5° subregions of the North Atlantic, eastern North Pacific, and western North Pacific tropical basins is developed. This product uses environmental and convective parameters computed from best-track tropical cyclone (TC) positions, National Centers for Environmental Prediction (NCEP) Global Forecasting System (GFS) analysis fields, and water vapor (~6.7 μm wavelength) imagery from multiple geostationary satellite platforms. The parameters are used in a two-step algorithm applied to the developmental dataset. First, a screening step removes all data points with environmental conditions highly unfavorable to TC formation. Then, a linear discriminant analysis (LDA) is applied to the screened dataset. A probabilistic prediction scheme for TC formation is developed from the results of the LDA.

Coefficients computed by the LDA show that the largest contributors to TC formation probability are climatology, 850-hPa circulation, and distance to an existing TC. The product was evaluated by its Brier and relative operating characteristic skill scores and reliability diagrams. These measures show that the algorithm-generated probabilistic forecasts are skillful with respect to climatology, and that there is relatively good agreement between forecast probabilities and observed frequencies. As such, this prediction scheme has been implemented as an operational product called the National Environmental Satellite, Data, and Information Services (NESDIS) Tropical Cyclone Formation Probability (TCFP) product. The TCFP product updates every 6 h and displays plots of TC formation probability and input parameter values on its Web site. At present, the TCFP provides real-time, objective TC formation guidance used by tropical cyclone forecast offices in the Atlantic, eastern Pacific, and western Pacific basins.

1. Introduction

Beginning in 2003, the National Hurricane Center (NHC) extended their official tropical cyclone (TC) track and intensity forecasts from 3 to 5 days, based upon the need for longer lead times. As forecasts are extended, it becomes increasingly possible for storms to form after the start of and have an impact before the end of a forecast period, intensifying the need for TC formation guidance. Currently, the NHC has an operational requirement to provide TC formation forecasts in its tropical weather outlooks. Other TC forecast centers such as the Joint Typhoon Warning Center and the Central Pacific Hurricane Center have similar requirements. Although subjectively generated, these forecasts rely heavily on various forms of objective guidance.

At this time, the most widely used source for TC formation guidance is global numerical models. As the resolution of global models increases, so does their promise in predicting TC formation (Pasch et al. 2006; Harr 2007). Yet uncertainty regarding their demonstrated forecast skill and model-based biases, including the tendency of these models to overpredict TC formation (Beven 1999), still limits their utility in TC forecasting. For these reasons, new objective methods of estimating TC formation probability are still desired.

Tropical cyclone formation is a rare event, and hence forecasting its likelihood on subbasin scales is a

Corresponding author address: Andrea Schumacher, CIRA–Colorado State University, Foothills Campus Delivery 1375, Fort Collins, CO 80523-1375.
E-mail: schumacher@cira.colostate.edu

DOI: 10.1175/2008WAF2007109.1

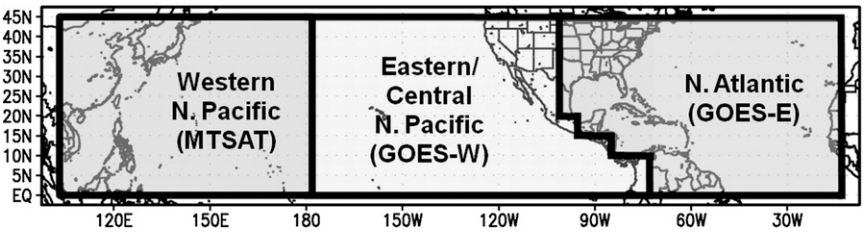

FIG. 1. The three basins covered by the TC formation product: the western North Pacific, eastern–central North Pacific, and Atlantic.

challenging task. To illustrate this point, consider the Atlantic tropical cyclone basin as defined in Fig. 1. There are 148 subregions of 5° × 5° latitude–longitude within this basin and 183 days in the official Atlantic hurricane season (1 June–30 November). During the period of 1949–2005, there was an average of 10.5 formations per year over the Atlantic basin. Thus, in any given 5° × 5° subregion, there is less than a 1 in 2579 chance (0.039%) of a TC forming within any given 24-h period. A similar analysis performed for the eastern and western North Pacific basins yields TC formation probabilities of 0.051% and 0.101%, respectively.

This ''needle in a haystack'' problem has received much attention over the years, and identifying and understanding the environmental conditions necessary for TC formation has been the topic of numerous studies. For example, Riehl (1948) studied TC formation in the North Pacific and found the upper-level disturbances in the vicinity of the low-level trades tended to enhance low-level instability, which can lead to TC formation. The global observational study of Gray (1968) noted that TCs tend to form in regions of weak vertical shear of the horizontal winds, which has been confirmed by others (e.g., Gray 1984; McBride and Zehr 1981; Bracken and Bosart 2000). Palmén (1948) discussed the link between TC formation and sea surface temperature (SST) and concluded that TCs typically form in regions where the SST exceeds 26°C. It has been shown that dry air at midlevels, via its entrainment into convective updraft cores and subsequent reduction in both buoyancy and precipitation efficiency (Ruprecht and Gray 1974; Gray 1975; Bister and Emanuel 1997), can inhibit sustained deep convection and have a negative effect on TC formation. Furthermore, the explicit role of tropical convection in TC formation has received considerable attention. Research in this area has spanned various spatial scales, including large-scale factors such as convective instability (Gray 1975; Ooyama 1990; DeMaria et al. 2001) and the intertropical convergence zone (ITCZ), the development of TCs from mesoscale disturbances such as easterly waves and midlevel convective vortices in the presence of deep convective bursts (McBride and Zehr 1981; Zehr 1992), and convective-scale features such as individual ''hot towers'' (Simpson et al. 1998) and their associated thermodynamic and dynamic anomalies [e.g., ''vortical hot towers''; Hendricks et al. (2004); Montgomery et al. (2006); Hendricks and Montgomery (2006)] .

Many of these findings have been incorporated into parameters for predicting TC formation. Gray (1975) created a seasonal genesis frequency parameter for the western North Pacific basin that was defined by the multiplicative combination of six primary genesis parameters: vertical shear, Coriolis parameter, low-level vorticity, sea surface temperature, moist stability, and midlevel relative humidity. This work was later expanded to a global framework (Gray 1979). The climatological values of this genesis frequency parameter were shown to be well correlated with observed TC formation (McBride 1995). Expanding on this approach, Emanuel and Nolan (2004) created a similar index that was more applicable to global climate model output. Similarly, DeMaria et al. (2001) developed a tropical cyclone genesis parameter (GP) for the tropical Atlantic basin that relied on 5-day running means of vertical shear, vertical instability, and midlevel moisture. They found that variations in the individual parameter inputs and the subsequent changes in GP helped to explain intra- and interseasonal variations in TC formation.

Perrone and Lowe (1986, hereafter PL86) and Hennon and Hobgood (2003, hereafter HH03) took a more focused approach by developing TC formation prediction schemes for use with tropical cloud clusters. Both studies developed algorithms using a statistical technique known as linear discriminant analysis (LDA) to determine which tropical cloud clusters would develop into tropical cyclones. PL86 used Navy Fleet Numerical Oceanography Central (NFNOC) analyzed archive fields and a step-wise discriminant analysis routine to develop a statistical forecast algorithm for TC genesis in the western North Pacific, and found

that the algorithm possessed skill when compared to climatology. The algorithm developed in HH03 analyzed a 3-yr sample (1998–2000) of developing and nondeveloping cloud clusters in the tropical North Atlantic that were subjectively identified from geostationary satellite infrared imagery. HH03 used environmental data from the National Centers for Environmental Prediction–National Center for Atmospheric Research (NCEP–NCAR) reanalysis fields (Kalnay et al. 1996) and applied a discriminant analysis much like that used by PL86. Like PL86, they too found that their discriminant analysis technique displayed skill at predicting TC formation from preexisting tropical cloud clusters.

In this paper, the approaches of PL86 and HH03 are generalized to develop a tropical cyclone formation probability scheme for real-time use over multiple tropical basins. A linear discriminant analysis is applied to the NCEP Global Forecasting System (GFS) model analysis fields and water vapor (6.7 μm) imagery from several geostationary satellites covering the North Atlantic, eastern North Pacific, and western North Pacific tropical cyclone basins. However, unlike PL86 and HH03, this study uses convective parameters in combination with environmental parameters in lieu of limiting analysis to existing tropical cloud clusters. Removing the need for subjective identification of cloud clusters allows for the development of an objective, spatially and temporally continuous product for estimating TC formation probability over an extended analysis domain.

Section 2 provides a description of the datasets used in this study. Section 3 describes the algorithm development and section 4 provides a statistical evaluation of the algorithm over dependent and independent datasets. The operational product that has been developed and implemented from the algorithm is described in section 5. Section 6 summarizes the results of this study and discusses plans for future work.

2. Datasets

The purpose of this study is to provide a new objective product for estimating the probability of tropical cyclone formation in the National Hurricane Center (NHC), Central Pacific Hurricane Center (CPHC), and Joint Typhoon Warning Center (JTWC) regions of forecast responsibility. The analysis domain extends from the equator to 45°N and from 100°E to 10°W, which covers all of the NHC and CPHC areas of responsibility and a portion of the JTWC area of responsibility. The analysis domain consists of three basins: the Atlantic, eastern Pacific and western Pacific, whose boundaries are determined by geostationary satellite coverage and agency responsibility (Fig. 1). The analysis domain is broken down into 5° × 5° latitude–longitude subregions,[1] which divide the domain into a set of 50 × 9 = 450 grid boxes. Environmental and convective parameters and formation probabilities are calculated over each of these subregions every 6 h at 0000, 0600, 1200, and 1800 UTC.

Information regarding historical tropical cyclone formation frequencies and locations was obtained from archived best-track files supplied by the NHC, CPHC, and JTWC. Each basin's best tracks from 1949 to 2005 were merged and reconciled for duplicate storm entries. For the purpose of this study, TC formation (or genesis) was defined as the first time and position in the best tracks when a storm was classified as a tropical system. System types included in the archived best tracks that are deemed tropical under this classification scheme include tropical depressions, tropical storms, and hurricanes/typhoons, while subtropical storms and extratropical storms are excluded. Track and intensity information for unnamed tropical depressions are not recorded in the official best tracks. For this reason, information on unnamed tropical depressions was obtained from the Automated Tropical Cyclone Forecast System (ATCF; Sampson and Schrader 2000). The ATCF was implemented in 1988, so unnamed tropical depression tracks were included from 1989 to 2005. The locations of all TC genesis cases included in the analysis dataset are shown in Fig. 2.

Monthly climatological TC formation probabilities were calculated by adding up the total number of TC formations in each subregion for each month over the 1949–2005 dataset and then dividing by the number of years (57). Figure 3 shows monthly climatological TC formation probabilities over the analysis domain for the month of September. The largest monthly TC formation probability occurs in September between 15°–20°N and 105°–110°W in the eastern Pacific basin (red grid box in Fig. 3). This value represents 31 TC formations that have occurred in that subregion during the month of September from 1949 to 2005, giving a monthly formation probability of 54.4% and hence an average daily formation probability of 1.8%. This climatological TC formation probability is relatively small, especially for the region with the highest number of TC formations per unit area in the world, which once again demonstrates the needle-in-a-haystack nature of predicting TC formation.

Environmental conditions within each subregion were determined using GFS analysis and reanalysis data. Prior to 2001, the NCAR–NCEP reanalysis fields,

[1] Hereafter, any reference to "subregions" is referring this defined set of 5° × 5° latitude–longitude grid boxes.

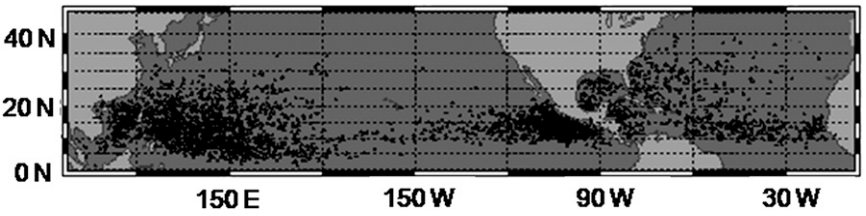

FIG. 2. All tropical cyclone formation points from the 1949–2005 best tracks.

available on a 2.5° × 2.5° global grid, were used. From 2001 to 2005, the NCEP global operational analysis data fields, available on a 1° × 1° global grid, were used. Both datasets were interpolated to a uniform global 2° × 2° grid.

In addition to the GFS data fields, water vapor (6.7 μm) imagery from geostationary satellites was used to calculate parameters related to deep convective activity. Since the analysis domain is too large to be covered by a single geostationary satellite, imagery from three currently operational geostationary satellites is needed to cover the analysis domain: *Geostationary Operational Environmental Satellite-E* (*GOES-E*, centered at 75°W), *GOES-W* (centered at 135°W), and *Multifunctional Transport Satellites-1R* (*MTSAT-1R*, centered at 140°E). Full-disk images from *GOES-E* and *GOES-W* were available back to 1995 and 1998, respectively, from the Cooperative Institute for Research in the Atmosphere (CIRA) satellite archives and the National Oceanic and Atmospheric Administration (NOAA) Comprehensive Large Array-Data Stewardship System (CLASS). Imagery from *MTSAT-1R* was obtained from CIRA archives dating back to November of 2005. Prior to November 2005, the region currently covered by *MTSAT-1R* was covered by *GOES-9* (centered at 155°E) and *Geostationary Meteorological Satellite-05* (*GMS-05*, centered at 140°E). Imagery from *GOES-9* was obtained for April 2003–November 2005 from NOAA CLASS and imagery for *GMS-05* dating back to 2000 was obtained from the Tropical Regional and Mesoscale Meteorology Branch (RAMM) Advanced Meteorological Satellite Demonstration and Interpretation System (RAMSDIS) archives at CIRA.[2] A summary of the geostationary satellite water vapor imagery sources collected for this study is shown in Fig. 4. All water vapor imagery was obtained from full-disk scans and was remapped to a 16-km Mercator projection prior to analysis. The Levitus climatological monthly SSTs (Levitus 1982) were also used.

The only cases included in this analysis were those for which both model reanalysis and satellite water vapor imagery were available. The NCEP–NCAR model reanalyses were available back to 1980, making satellite data availability the limiting factor. Hence, the analysis time periods for the Atlantic, eastern Pacific, and western Pacific basins extend from 1995, 1998, and 2000 to 2005, respectively.

3. Algorithm development

The algorithm developed here is similar to that of Knaff et al. (2008, hereafter K08). The K08 procedure involved two steps—a screening step and then a linear discriminant analysis step—that used environmental values from satellite infrared imagery and analyses from the Statistical Hurricane Intensity Prediction Scheme (SHIPS; DeMaria et al. 2005) model to identify a subset of tropical cyclones known as annular hurricanes. Since the present study also seeks to discriminate between two groups—TC formation and nonformation cases—based on environmental conditions, the same two-step methodology is used. The first step involves screening out all sample set data points for which tropical cyclone formation is highly unlikely. The second step involves the use of a linear discriminant analysis (see Wilks 2006), which allows one to distinguish between two groups on the basis of a k-dimensional vector of observations, $\mathbf{x}$. In this case, $\mathbf{x}$ represents a list of environmental and convective parameters expected to have relationships with TC formation.

K08 assesses the effectiveness of its algorithm by evaluating hit rates and false alarm rates. Given the similarities of our analysis methods, we will use the same strategy where applicable. These metrics rely on four quantities that can be obtained from a standard 2 × 2 contingency table as described in Wilks (2006) and has been reproduced in Table 1. In this table, a is the number of observed TC formation events that were forecasted as formation events by the algorithm (i.e., ''hits''), b is the number of observed nonformation events that were forecasted as formation events by the algorithm (i.e., ''false alarms''), c is the number of observed formation events that were forecasted as nonformation events by the algorithm (i.e., ''misses''), and d

[2] Tropical RAMSDIS archives only included satellite imagery from May to November.

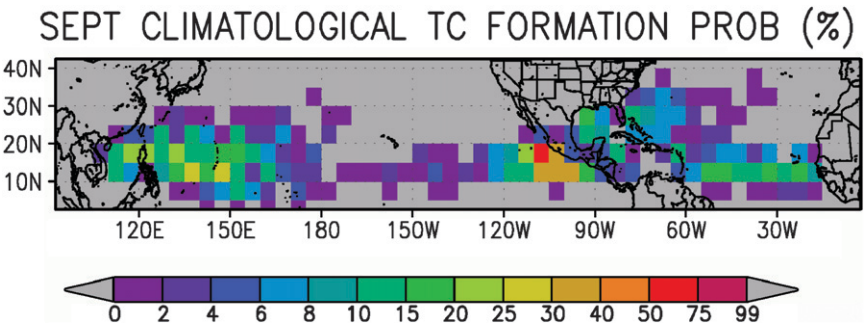

FIG. 3. Climatological TC formation probabilities for the month of September, calculated from the 1949–2005 best tracks.

is the number of observed nonformation events that were forecasted as nonformation events (i.e., "correct negatives"). Following this convention of Wilks (2006), the hit rate, which is also commonly referred to as the probability of detection, is defined as HR = $a/(a + c)$. The false alarm rate is defined as FAR = $b/(b + d)$.

a. Environmental parameters

Before either step of the algorithm could begin, a set of environmental and convective parameters had to be chosen. As described in section 1, numerous environmental conditions have been found to have an effect on TC formation. Input parameters were taken from the more robust results of TC formation research, and only those values that were calculable on subregional scales from the available datasets were used. The input parameters chosen for this study are 850–200-hPa vertical shear (VSHEAR), 850-hPa circulation (CIRC), vertical instability (THDEV), 850-hPa horizontal divergence (HDIV), latitude (LAT), percent land coverage (PLAND), distance to any existing TC (DSTRM), climatological SST (CSST), cloud-cleared water vapor brightness temperature (BTWARM), percentage of cold pixel coverage (PCCOLD), and 24-h climatological TC formation probability (CPROB). Additional information on parameter choices and methods of calculation is provided in the appendix.

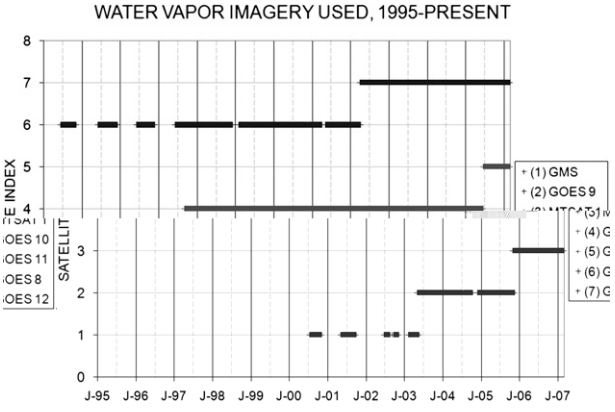

FIG. 4. Inventory of water vapor imagery from geostationary satellites used in the analysis. The abscissa labels correspond to 1 January of each year (e.g., J-98 stands for 1 Jan 1998). The ordinate labels are index values that correspond to the numbers shown to the left of each geostationary satellite listed in the legend. Satellite indices 1–3 represent western Pacific satellite coverage, 4–5 represent eastern Pacific satellite coverage, and 6–7 represent Atlantic satellite coverage.

b. Screening step

The first step of the algorithm consists of screening out all cases for which TC formation is highly unlikely. Although the parameters chosen for this study influence TC formation in all regions of the analysis domain, the relative magnitudes of these influences may vary from basin to basin. For this reason each basin was treated as an independent dataset during algorithm development. The same procedure, described here, was applied to each basin individually.

To determine the appropriate screening thresholds, all cases in the developmental dataset were partitioned into two groups: TC genesis (TCG) and no TC genesis (NTCG). Here, a "case" refers to any given 5° × 5° latitude–longitude subregion at a single analysis time of 0000, 0600, 1200, or 1800 UTC. When a tropical cyclone forms, all cases spatially coincident with the formation location at times within 24 h prior to the formation time are assigned to the TCG group. Since the analysis is

TABLE 1. The 2 × 2 contingency table values, as defined in Wilks (2006).

		Observed	
		Yes	No
Forecast	Yes	*a* (hits)	*b* (false alarms)
	No	*c* (misses)	*d* (correct negatives)

TABLE 2. The criteria used to eliminate data points from the dataset during the screening step. Note that CPROB was not used for screening because it is derived from a limited best track dataset (1949–2005). In the third column, NCEP indicates the data source is the NCEP GFS analyses and SAT WV indicates the data source is satellite water vapor (6.7 μm) imagery.

Abbreviation	Screening parameter	Data source	Elimination criteria		
			Atlantic	Eastern Pacific	Western Pacific
LAT	Lat (°N)	Domain definition	<5.0	<5.0	<5.0
PLAND	Land coverage (%)	Land mask	≥100.0	≥100.0	≥100.0
DSTRM	Distance to nearest TC (° lat–lon)	Best tracks	<2.5	<2.5	<2.5
CSST	Max climatological SST (°C)	Levitus SST	<21.0	<21.0	<21.0
VSHEAR	200–850-hPa vertical shear (m s^{-1})	NCEP	>25.2	>15.9	>19.5
CIRC	850-hPa circulation (m s^{-1})	NCEP	<−1.5	<−1.2	<−0.9
THDEV	Vertical instability (°C)	NCEP	<−2.6	<−3.0	<1.6
HDIV	850-hPa horizontal divergence ($\times 10^{-5}$ s^{-1})	NCEP	>1.0	>0.7	>0.5
PCCOLD	Cold pixel count (%)	SAT WV	<2.8	<5.0	<3.0
BTWARM	Avg cloud-cleared brightness temperature (°C)	SAT WV	>−25.4	>−23.1	>−27.8

performed at 6-h intervals, each TC formation in the best-track record represents four TCG cases in the developmental dataset. All cases not assigned to the TCG group were considered NTCG cases.

The only parameter listed in section 3a not used for screening is CPROB. This value is computed from a finite (57 yr) record. As such, when a subregion has a value of CPROB = 0, it does not necessarily imply that tropical cyclone formation is highly unlikely, but rather indicates that a tropical cyclone has not occurred at that particular place and time in the last 57 yr. The lack of a physical relationship between CPROB and TC formation along with the limited nature of the climatological dataset make it unsuitable for use as a screening parameter. The range of parameter values for each group was examined, and screening criteria were defined so that no more than 1% of TCG cases were removed by any one parameter's screening criterion. With 10 screening criteria, this method guarantees that a maximum of 10% of TCG cases would be eliminated from the analysis dataset. The final criteria chosen (Table 2) eliminated approximately 5% of TCG cases in each basin while 76%, 89%, and 75% of NTCG cases were eliminated from the Atlantic, eastern Pacific, and western Pacific datasets, respectively (Table 3, first two rows).

If we were to evaluate the screening step alone as a forecast, where all data points screened out are equivalent to a forecast of NTCG and all points retained are considered TCG forecasts, we could compute the corresponding hit rates and false alarm rates described at the beginning of this section. Doing so, the screening step results in hit rates of 95%, 95%, and 96%, and false alarm rates of 24%, 11%, and 25% for the Atlantic, eastern Pacific, and western Pacific basins, respectively. Although the hit rates are high by design, the false alarm rates in conjunction with the large number of NTCG data points left in the sample set make screening alone an ineffective predictor of TCG. For example, in the Atlantic there are 701 TCG cases and 1 818 983 NTCG cases in the development dataset. A hit rate of 95% corresponds to 665 correctly identified TCG cases. To compare, a false alarm rate of 24% corresponds to 428 553 false alarms. This results in a TC formation probability of 100 × (665/428 553) = 0.16%. Although screening results in a probability that is a fourfold improvement over the 0.039% random probability computed in section 1, the staggering number of false alarms in relation to hits makes screening alone ineffective for the purposes of forecasting TC formation.

c. *Linear discriminant analysis step*

To improve the skill of our algorithm over that provided by screening alone, LDA (Wilks 2006) was applied to the screened developmental dataset. This procedure uses the parameter values and group membership (i.e., TCG or NTCG cases) of each case in the developmental dataset to solve for a set of coefficients that can be used to determine the group membership of independent data points. In other words, for any independent data point with parameter values $x_1, x_2, \ldots, x_n$, the discriminant function is

$$f = a_0 + \sum_{i=1}^{n} a_i x_i,$$

where n is the number of parameters and a_0 is a constant term. This function can be used to determine if the point is a TCG (NTCG) case depending on whether $f > 0$ ($f < 0$). The LDA calculates the coefficient values $a_1, a_2, \ldots, a_n$ so that the distances between the mean parameter values for groups of TCG cases and NTCG cases are maximized in standard deviation units.

Not all of the parameters listed in section 3a were used as LDA inputs. Although there is no strict independence requirement for LDA input parameters, both

TABLE 3. The 2 × 2 contingency tables for an idealized forecast from Wilks (2006) (first column) and for the Atlantic basin (second column), eastern Pacific basin (third column), and western Pacific basin (fourth column) after the screening step (first two rows) and after the combined screening step and LDA step (last two rows).

			Wilks (2006)		Atlantic		Eastern Pacific		Western Pacific	
			Observed		Observed		Observed		Observed	
			Yes	No	Yes	No	Yes	No	Yes	No
Screening step	Forecast	Yes	*a*	*b*	665	428 553	479	174 660	476	183 188
		No	*c*	*d*	36	1 390 430	26	1 462 263	22	553 636
Screening + LDA step	Forecast	Yes	*a*	*b*	99	1673	115	1326	43	297
		No	*c*	*d*	602	1 817 310	390	1 635 597	455	736 527

LAT and CSST were omitted because their contributions were already captured in the climatological formation probability parameter, CPROB. In addition, results from an initial LDA showed that THDEV and BTWARM have relatively weak contributions to the discriminant function. This agrees with Molinari et al. (2000), who suggested that the thermodynamic conditions (in the eastern Pacific basin) are sufficient in most places most of the time, and that the best predictors of TCG are those associated with an initial disturbance. Hence, the thermodynamic predictors of BTWARM and THDEV were not used in the final LDA. This left seven discriminating parameters: PLAND, DSTRM, CPROB, VSHEAR, CIRC, HDIV, and PCCOLD.

Applying LDA yielded a set of seven discriminant coefficients, whose standardized values (i.e., the pooled standard deviation for each input parameter times the corresponding coefficient) are shown in Table 4. The standardized discriminant coefficients represent the magnitude of each input parameter's contribution to the discriminant function value. Table 4 shows that the parameters contributing the most to the discriminant function values are CPROB, CIRC, and DSTRM. For the Atlantic and eastern Pacific basins, the highest contribution comes from CPROB, then CIRC, followed by DSTRM. The large contribution by CPROB suggests that these basins each have relatively consistent climatological patterns of TCG location and timing. This holds especially true for the eastern Pacific basin, which has the highest frequency of TCG per unit area of any region worldwide (Elsberry et al. 1987). In the western Pacific, CPROB is the third largest contributor, suggesting that the timing and location of TC formation regions may vary more within a given season than in the other two basins. This may be due to the large intra- and interseasonal variations in the strength and location of the monsoon trough in the western Pacific as compared to the eastern Pacific, which is strongly tied to TC formation in both of those basins (Briegel and Frank 1997).

TABLE 4. Standardized discriminant coefficients for each parameter in each basin, derived from linear discriminant analysis after screening.

	Atlantic	Eastern Pacific	Western Pacific
PLAND	−0.21	−0.27	−0.20
CPROB	1.47	1.67	0.88
VSHEAR	−0.36	−0.22	−0.17
CIRC	1.32	1.41	1.59
PCCOLD	0.62	0.29	0.55
HDIV	−0.22	−0.39	−0.33
DSTRM	0.75	0.67	1.14

The strong contribution by CIRC is consistent with the idea that an initial disturbance is necessary for TC formation. Results from two recent studies by Frank and Roundy (2006) and Davis et al. (2007) also support this idea. Frank and Roundy (2006) demonstrated a strong relationship between TC formation and several types of atmospheric waves. They suggested a forcing mechanism whereby waves enhance local circulations, which in turn promote TC formation. Davis et al. (2007) studied vortices in the eastern Pacific and found that those that eventually developed into tropical cyclones tended to be stronger and deeper from the outset as compared to nondeveloping vortices, once again suggesting a correlation between positive low-level circulation and subsequent TC development.

At first, the finding that DSTRM is a strong contributor to TC formation likelihood was unexpected. This is especially true in light of the finding that VSHEAR had a much smaller contribution to TC formation probability than many parameters, despite the considerable attention it has received in TC formation research. It is known that a large amount of vertical shear is detrimental to TC genesis (Riehl 1948) while a little bit of vertical shear may be helpful (McBride and Zehr 1981; Bracken and Bosart 2000). However, it is still not known if variations in intermediate values of shear are important to TC formation like they are to TC intensity change. The relatively small contribution of VSHEAR in this analysis suggests that the predictive relationship

between vertical shear and TC formation is either too weak or too complex to project significantly on the LDA. However, it is well known that large amounts of vertical shear, such as the shear induced by an existing TC, have a negative effect on TC formation. Combined with the effects of storm-induced upwelling and SST cooling, the local environment of an existing TC is generally unfavorable for new TC formation. These negative impacts are relatively localized about the existing TC and will decrease with distance, which would explain the relatively large positive values of the standardized discriminant coefficients for DSTRM.

LDA produces a binary classification scheme that designates each data point as being a TCG or NTCG case. Binary classification schemes can be evaluated using hit rates and false alarm rates, which are shown for the combined screening step and LDA step in the last two rows of Table 3. The LDA step leads to a decrease in the number of TCG cases correctly identified by at least a factor of 4. This results in a reduction of hits rates from values ranging from 94% to 95% to values as low as 9%, suggesting that the LDA step greatly reduces the algorithm's ability to identify TCG occurrences. However, the number of NTCG cases mistakenly identified as TCG cases (i.e., false alarms) by the algorithm dropped even more drastically, reducing false alarm rates from 10%–25% to 0.04–0.09%. In the case of this extremely rare occurrence, the large reduction in false alarm rates outweighs the lesser reduction in hit rates, making LDA an important step in generating a useful TC formation prediction scheme.

For this project, a probabilistic scheme is sought for estimating TC formation likelihood. This probabilistic scheme was created from the results of the LDA by partitioning the TCG cases into 10 subgroups of equal size based on their discriminant values, whose values define 10 discriminant value intervals. The TC formation occurrence frequencies were then calculated for each interval and used as TC formation probabilities. So, for any given independent data point, the corresponding discriminant value is linearly interpolated[3] to obtain a formation probability, thus generating a probabilistic forecast. The next section will evaluate the performance of this algorithm using statistical forecast verification methods.

[3] The linear interpolation scheme introduced a bias toward overprediction in each basin. To correct for this bias, each probability is multiplied by the scaling factor S_o/S_p, where S_p is the summation of the algorithm-predicted probabilities over all dependent data points and S_o is the summation of all observed TC cases within the dependent dataset. Note that the scaling factor was calculated and applied independently for each of the three basins.

4. Algorithm verification

The algorithm developed in this study provides a probabilistic, short-term forecast of tropical cyclone formation. Since TC formation is an extremely rare event, the typical statistical verification methods that would be applied to a probabilistic forecast have biases that make many of them insufficient for estimating skill. For example, consider that for a probability threshold $p = 0.4\%$ chosen for the Atlantic basin, the corresponding hit rate and false alarm rate are HR = 65.2% and FAR = 2.3%. These values are not far off from those reported in HH03 and PL86, and at face value appear to suggest a skillful forecast. However, with 428 553 NTCG cases in the Atlantic dataset, this equates to more than 9800 false alarms. Within the generalized framework of this analysis TC genesis is an *extremely* rare occurrence, which makes is difficult to compare existing results that rely on restricted initial sample sets. As such, we will attempt to define an appropriate methodology for evaluating the skill of our TC formation estimation scheme.

Although standard verification measures for probabilistic forecasts are not suitable for use with extremely rare events, there are some variations of these metrics that compare the performance of a forecast to that of a reference forecast to determine skill. The best available reference forecasts in this case are the null forecast (assuming $p = 0\%$ everywhere) and CPROB. For each verification measure used, it was found that the climatological formation probability forecast performed better than the null forecast. As such, climatology was used as the reference forecast for each skill score computed in the following sections. The results of each verification method are given for both the dependent (1995–2005) and independent (2006–07) datasets.

a. Brier skill score

The first verification diagnostic used was the Brier skill score, $\mathrm{BSS} = 1 - (\mathrm{BS}/\mathrm{BS}_{\mathrm{ref}})$, where BS is the Brier score of the algorithm and $\mathrm{BS}_{\mathrm{ref}}$ is a reference Brier score (Murphy 1973). The Brier score, as defined by Wilks (2006), is

$$\mathrm{BS} = 1/n \sum_{k=1,n} (y_k - o_k)^2,$$

where y_k and o_k are the predicted and observed probabilities for case k, respectively, and n is the number of forecast–event pairs. The Brier score is essentially the mean squared error of the probability forecasts (Wilks 2006). The BSS is a measure of the improvement of a probabilistic forecast over the reference forecast and

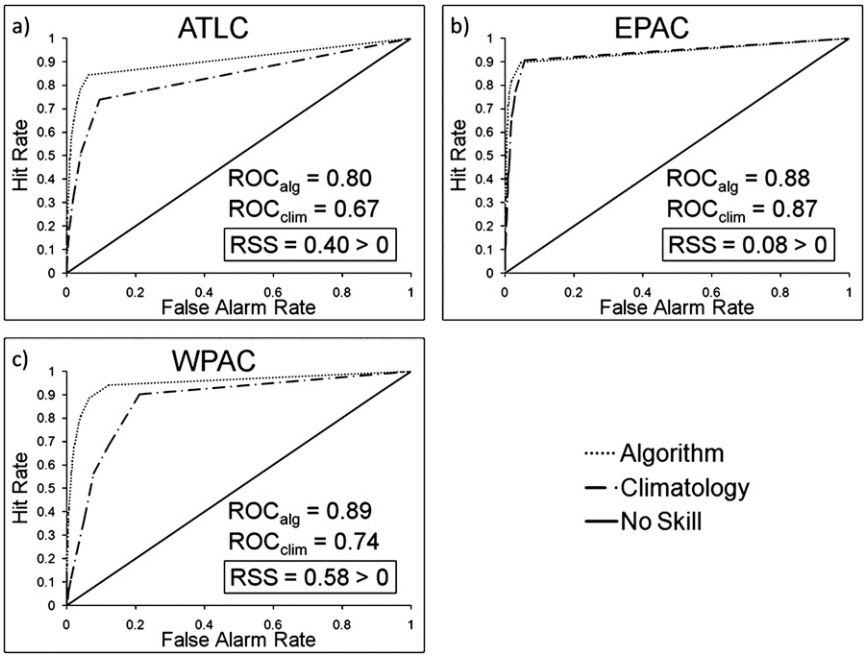

FIG. 5. ROC plots for the (a) Atlantic, (b) eastern Pacific, and (c) western Pacific basins over the dependent dataset.

can range from $-\infty$ to 1, with 0 indicating no skill with respect to the reference forecast and 1 being a perfect score. When the climatological formation probability is used for BS_{ref}, the BSS for the dependent years are 0.012, 0.024, and 0.025 for the Atlantic, eastern Pacific, and western Pacific basins, respectively. The corresponding independent years' BSSs are 0.006, 0.023, and 0.017, respectively. Although the BSS values are relatively small, they are all positive, which indicates that the algorithm provides a more skillful forecast than climatology alone.

b. Relative operating characteristic skill score

Another gauge of forecast skill that can be used for this scheme is the relative operating characteristic (ROC). A ROC diagram is created by plotting the hit rate versus the false alarm rate using a set of increasing probability thresholds to make the yes–no decision (Mason and Graham 1999; Wilks 2006). The area under the resultant curve is the ROC value and provides information regarding the ability of a forecast to discriminate between events and nonevents. ROC values can range from 0 to 1, where a score of 0.5 or less indicates no skill and a score of 1 is perfect. The ROC values for dependent years for the Atlantic, eastern Pacific, and western Pacific basins are 0.80, 0.88, and 0.89, respectively (Fig. 5). As discussed at the beginning of this section, these scores alone are not necessarily representative of the overall forecast skill of the algorithm, due to known problems with using the ROC for extremely rare events (Stephenson 2004). Hence, for verification purposes we will look at the ROC skill score (SS_{ROC}), which is defined in Wilks (2006) as $SS_{ROC} = (ROC_{alg} - ROC_{ref})/(ROC_{perf} - ROC_{ref})$, where ROC_{alg} is the ROC value of the product algorithm, ROC_{ref} is the ROC value of the reference forecast (in this case climatology), and ROC_{perf} is the ROC value corresponding to a perfect forecast, which in this case is equal to 1. Like the Brier skill score, a perfect score is 1 with an $SS_{ROC} > 0$ indicating the product forecast has skill with respect to the reference forecast. The dependent years' SS_{ROC} values for the Atlantic, eastern Pacific, and western Pacific basins are 0.40, 0.08, and 0.58, respectively. The corresponding SS_{ROC} values for the independent years are 0.31, 0.45, and 0.33, respectively. Like the Brier skill score results, all of the SS_{ROC} values are positive, indicating the algorithm possesses skill over climatology alone.

c. Reliability diagrams

To determine how well the algorithm-estimated TC formation probabilities correspond to observed frequencies, the reliability diagrams for both the dependent and independent years were plotted. Reliability diagrams for both dependent and independent years for each basin are shown in Fig. 6. Each diagram includes a distribution plot showing the number of cases belonging to each probability bin. Examination of the diagrams for the

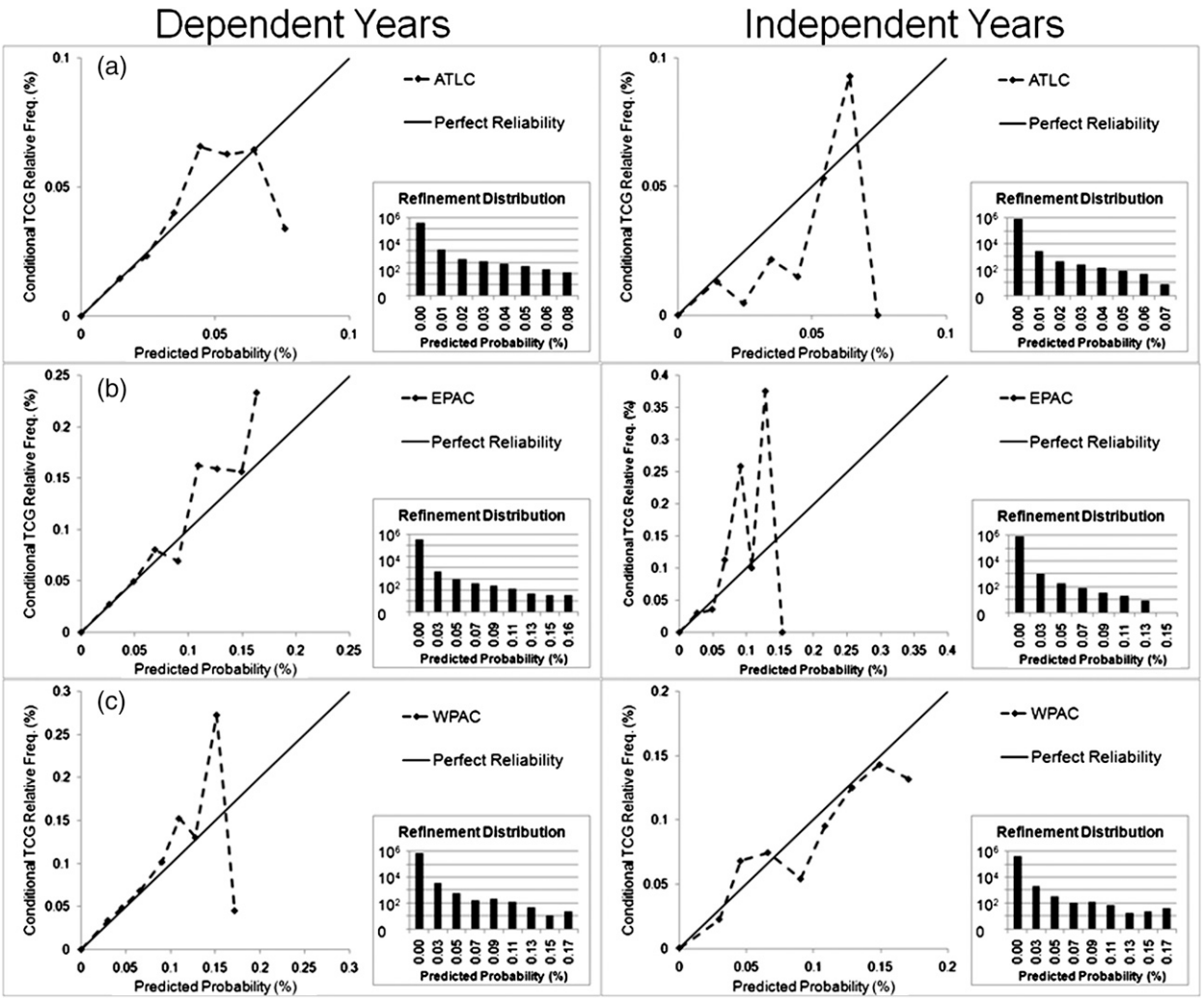

FIG. 6. Reliability diagrams for the (a) Atlantic, (b) eastern Pacific, and (c) western Pacific basins. Each plot shows reliability diagrams for (left) dependent years and (right) independent years.

dependent years shows that all three basins are generally well calibrated. There appears to be a slight conditional bias in the eastern Pacific toward underprediction of TC formation at higher predicted probabilities, and there may be hint of the same bias in both the Atlantic and western Pacific as well. The diagrams for the independent years indicate there was a bias toward overprediction in the Atlantic, a conditional bias toward underprediction in the eastern Pacific at higher probabilities, and good calibration and resolution in the western Pacific.

5. The NESDIS Tropical Cyclone Formation Probability product

The algorithm developed in this study has been implemented as the National Environmental Satellite, Data, and Information Services (NESDIS) Tropical Cyclone Formation Probability (TCFP) product, which is currently running in real time online (http://www.ssd.noaa.gov/PS/TROP/genesis.html). The TCFP product Web site includes a domain-wide overview plot indicating regions of elevated TC formation probability along with a corresponding enhanced water vapor loop. Each of the three basins has its own Web page that displays color contour *x*–*y* plots of real-time, climatological, and anomaly formation probability and predictor values (Fig. 7).

Each basin has been divided into a set of subbasins as shown in Fig. 8. To provide continuity over time, both the product-estimated and climatological formation probabilities (input parameter values) are summed (averaged) over each subbasin and displayed as time series plots. These time series are useful for identifying subbasin-scale variations in input parameter values and the corresponding changes in TC formation probability.

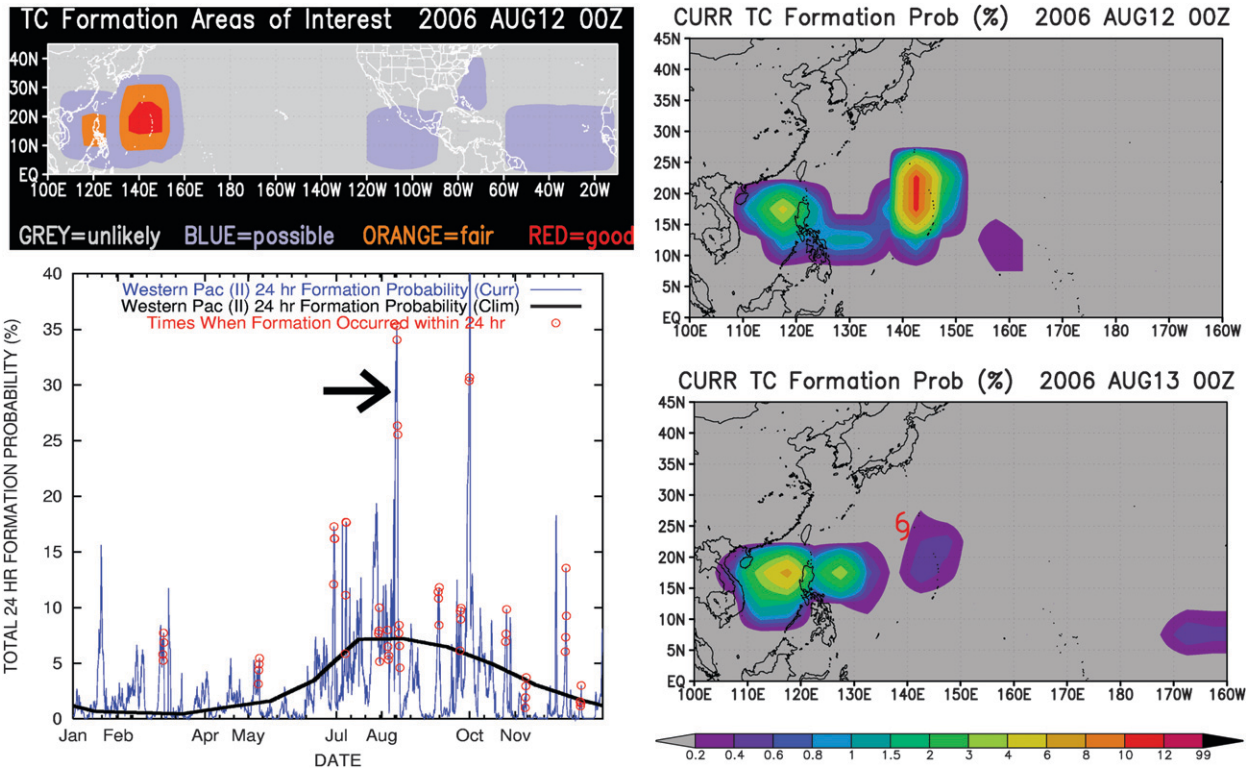

FIG. 7. Example of the TCFP product output during the formation of TS Wukong at 1200 UTC 12 Aug 2006. This includes (top left) the main Web page plot denoting areas of enhanced TC formation probability, the predicted TC formation probabilities for the western Pacific basin at (top right) 12 h prior to and (bottom right) 12 h after formation, and (bottom left) the time series plot of cumulative TC formation probability for subbasin WP2. Note that the arrow in the time series plot is pointing to the probability peak coincident with the formation of TS Wukong.

The time series plot of 24-h-predicted TC formation probability over the eastern Pacific (Fig. 8) subbasin is shown in Fig. 9. The red open circles in Fig. 9 represent the times within 24 h prior to observed TC formation. As Fig. 9 shows, most of the red open circles are coincident with peaks in subbasin summation TC formation probability. In fact, for the eastern Pacific subbasin from 1998 to 2005, 81.5% of the TCG points occur at times when the subbasin formation probability is greater than its climatological value and over half of the TCG points are coincident with a local maximum in the TC formation probability. It turns out that this result is robust over most subbasins, with 80.3% of the total TCG points occurring at times when the subbasin formation

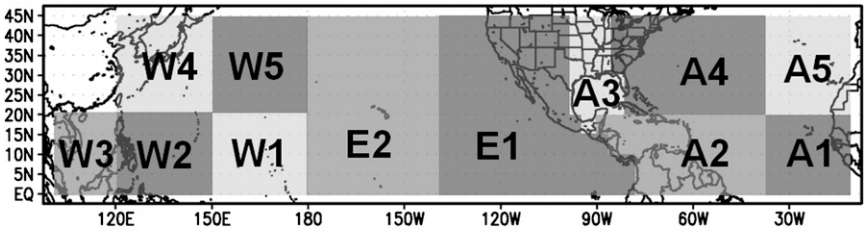

FIG. 8. The 12 TCFP subbasins.

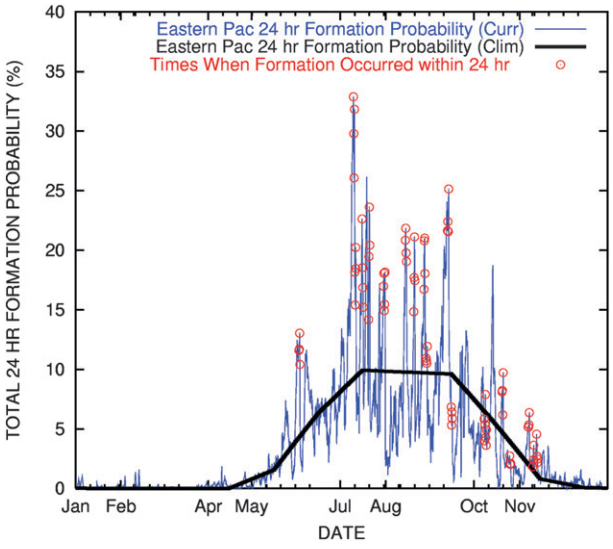

FIG. 9. Time series plot of 24-h product predicted TC formation probability (blue line), 24-h climatological TC formation probability (black line), and times when TC formation occurred within 24 h (red open circles) for the eastern Pacific subbasin in 2006.

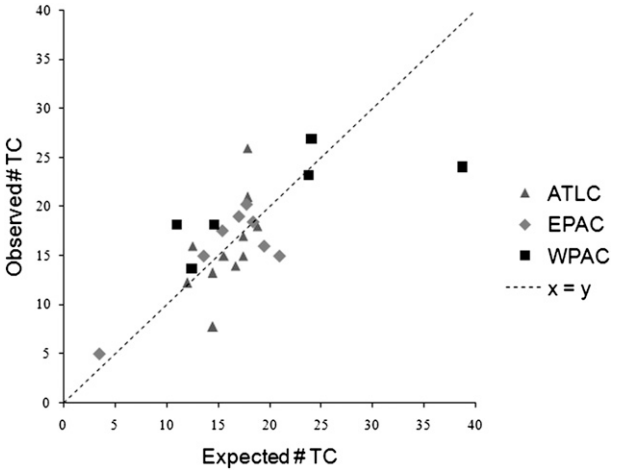

FIG. 10. Plot of expected vs observed number of TC formations for each year in the analysis dataset.

probability is greater than its climatological value. The fine resolution of the analysis grid introduces the problem of TCs moving in and out of grid boxes during the forecast period, which leads to a negative bias in algorithm hit rates. Using the subbasin summation of formation probability reduces this problem and gives a more representative view of formation probability when a region of increased TC formation probability spans a large region, such as in an active phase of the monsoon trough or an elongated easterly wave.

After examining subbasin averages and sums, it seems prudent to examine these probabilities on the basin scale. To do so, the product probabilities were summed over the entirety of each basin for each dependent and independent year and compared to the observed number of TC formations in that basin. The results from this computation are plotted in Fig. 10. Although the probabilities have been bias corrected so that the cumulative predicted probabilities equal the total number of TC observations over the dependent dataset, the difference between the predicted and actual number of TCs for individual years is apparent in Fig. 10. Most of the data points in Fig. 10 are relatively close to the $x = y$ line (dashed), indicating that the TCFP product is performing well on the annual, basin-wide scale.

6. Summary and future work

a. Summary

A product for estimating the 24-h probability of TC formation within each 5° × 5° latitude–longitude subregion in the Atlantic, eastern Pacific, and western Pacific tropical basins was developed. This product uses both environmental parameters from ATCF best tracks and NCEP GFS data fields as well as convective parameters from the *GOES-E*, *GOES-W*, and *MTSAT-1R* water vapor imagery. This algorithm was developed using a two-step process that involves 1) screening out data points where TC formation is highly unlikely and 2) linear discriminant analysis. The resultant discriminant function values are interpolated to 24-h TC formation probabilities.

Verification of the TCFP product, using both the Brier skill score and relative operating characteristic, showed that the product forecast possesses skill with respect to both the null hypothesis and climatology. Reliability diagrams also show the product estimated probabilities to have generally good calibration, with some bias toward underprediction in the eastern Pacific basin. Although individual product probability values are generally no greater than 10%–15%, they are a vast improvement on climatological values, which are on the order of 0.1%. In addition, the mean algorithm-derived 24-h TC formation probabilities for TCG cases are 1.5%, 3.0%, and 2.6% for the Atlantic, eastern Pacific, and western Pacific basins, respectively, while the corresponding means for the NTCG cases are 0.04%, 0.03%, and 0.07%. The differences between the group means were found to be significant at the 99% confidence level using the Student's t statistic.

b. Future work

Several different approaches for improving the TCFP product are currently being considered. The first involves extending the analysis domain to include the Indian Ocean and Southern Hemisphere tropical cyclone

basins, essentially making the product global. The real-time, objective TC formation guidance supplied by this product could be of use to meteorological agencies in these regions, including the JTWC; National Weather Service (NWS) offices in Pago Pago and American Samoa; the Fiji TC Regional Meteorological Specialized Center (RMSC); the La Reunion RMSC; and the Perth, Darwin, and Brisbane TC Warning Centres.

Another improvement involves identifying additional environmental parameters to add to the algorithm. Two such parameters being considered are the positions and Dvorak intensities for invest tropical systems supplied by the NCEP/TPC Tropical Analysis and Forecast Branch. Additionally, the current TCFP product determines the probability of TC formation within 24 h, which is a short forecast period. Future research will investigate ways in which the forecast period can be extended to 48 h and beyond. This may include the use of the GFS forecast fields in addition to the analyses. Also, Frank and Roundy (2006) demonstrated that TC formation is strongly related to several types of atmospheric waves and identified corresponding phase relationships. Given the fact that convective anomalies associated with these waves are detectable up to a month in advance of TC formation, the statistical TC formation forecasts developed by Frank and Roundy (2006) introduce the idea of using upstream convective parameters to extend the TCFP product forecast period. Work is currently under way to collect and analyze global geostationary satellite imagery for potential upstream wave–related convective signatures that can be incorporated into the current algorithm.

Acknowledgments. This work is supported by NOAA Grant NA17RJ1228. The authors thank Lixion Avila, Ed Rappaport, Chris Landsea, and Edward Fukada for providing motivation and guidance in developing this product; Bernadette Connell for supplying *GOES-West* water vapor imagery; and Ray Zehr for supplying *GMS-05* and *MTSAT-1R* water vapor imagery from the tropical RAMSDIS archives. The views, opinions, and findings in this report are those of the author and should not be construed as an official NOAA or U.S. government position, policy, or decision.

APPENDIX

Environmental and Convective Parameters

a. Latitude

Latitude can have an important impact on TC formation, particularly in terms of limiting its likelihood. Tropical cyclone formation is rare at low latitudes (Fig. 2), where the Coriolis parameter (and hence planetary vorticity) is nearly zero and surface winds (and hence pressure gradients) are generally weak (Gray 1975, 1979). For this study, the latitude (LAT) is defined at the center of each 5° × 5° latitude–longitude subregion.

b. Percent land

Energy fluxes between a tropical cyclone and the ocean surface play a crucial role in TC formation and intensification (Malkus and Riehl 1960; Leipper 1967; Gray 1975). For this reason, it is highly unlikely for a tropical cyclone to form over land (Fig. 2). For these reasons, the percent of each 5° × 5° latitude–longitude subregion over land (PLAND) was included as a parameter.

c. Distance to an existing tropical cyclone

An existing TC introduces storm-related vertical shear, changes the local atmospheric moisture content, and causes upwelling that decreases SST, all of which result in an environment that is unfavorable for new TC development. Analysis of the 1949–2005 best tracks confirms that in the last 57 yr, no TC has ever formed within 400 km of an existing TC, justifying the inclusion of this distance as a parameter. The distance from the center of each 5° × 5° latitude–longitude subregion to an existing TC (DSTRM) is calculated from the ATCF best-track positions for each analysis time. Since the effects of an existing TC are localized, variations in distances beyond 1000 km are not expected to have any predictive quality and hence all values of DSTRM greater than 1000 km are set equal to 1000 km.

d. Sea surface temperature

Shapiro and Goldenberg (1998) demonstrated that SSTs have a direct effect on enhancing TC formation. The exact threshold value for SSTs that support TCG is still unknown; however, Palmén (1948) suggested an SST of 26°C was needed to support tropical cyclone formation. SST, however, is expected to be highly correlated with the equivalent potential temperature at 850 hPa, which is a large contributor to the THEDEV parameter (see section g of this appendix). As such, the monthly Levitus climatological SST (Levitus 1982) values were used in this algorithm and were only employed for screening purposes. CSST was derived by linearly interpreting between these monthly values.

e. Vertical shear

In a study of western Pacific typhoons, Riehl (1948) found that TC formation can be inhibited by strong

vertical shear of the horizontal wind. In addition, several studies have suggested that some weak amount of vertical shear is necessary for TC development (e.g., McBride and Zehr 1981; Bracken and Bosart 2000). This relationship between vertical shear and TC formation was recognized by Gray (1968) and DeMaria et al. (2001), and was included as dynamical parameters in their respective TC genesis parameters. For this study, the magnitude of the vertical shear of the zonal wind (VSHEAR) is calculated from the GFS analysis horizontal wind fields for each subregion as

$$\text{VSHEAR} = \sqrt{(\overline{u_{850}} - \overline{u_{200}})^2 + (\overline{v_{850}} - \overline{v_{200}})^2},$$

where $\overline{u_{850}}$ ($\overline{v_{850}}$) and $\overline{u_{200}}$ ($\overline{v_{200}}$) are the zonal (meridional) winds at 850 hPa and 200 hPa, respectively, averaged over the 12° × 12° latitude–longitude GFS subgrid that is centered on the analysis subregion.

f. Low-level circulation

Gray (1968, 1975, 1979) noted tropical cyclones tend to form in regions of anomalous positive vorticity. The observational studies of Frank and Clark (1980), McBride and Zehr (1981), and others confirm the importance of low-level cyclonic circulation and vorticity in determining formation potential. This increase enhances the heat and moisture fluxes from the ocean surface and, in the presence of deep convective bursts, leads to the development of the low-level, warm-core TC vortex (Hendricks et al. 2004; Montgomery et al. 2006; Hendricks and Montgomery 2006). The 850-hPa circulation (CIRC) is calculated as the line integral of the 850-hPa GFS wind field over the perimeter of an 8° × 8° subgrid of the GFS data field that is centered on the algorithm subregion, so

$$\text{CIRC} = \oint_P \mathbf{U} \cdot dl,$$

where **U** is the average magnitude of the along-contour component of the horizontal wind field and P is the contour defined along the perimeter of the 8° × 8° subgrid.

g. Vertical instability

Vertical instability is needed to support the deep convective activity necessary for TC formation. The vertical instability parameter from DeMaria et al. (2001), which was developed using the parcel calculation formulation described in Ooyama (1990), is used in this study. Vertical instability (THDEV) is calculated for each subregion using the equation

$$\text{THDEV} = \sum_{p=850\ \text{hPa}}^{200\ \text{hPa}} \text{wt}(p)[\overline{\theta_E(850\ hPa)} - \overline{\theta_E^*(p)}],$$

where wt(p) is the pressure weighting, and $\overline{\theta_E}$ and $\overline{\theta_E^*}$ are the equivalent potential temperature and saturated equivalent potential temperature, respectively, averaged over a 8° × 8° subgrid of the GFS data field.

h. Low-level divergence

Several studies of TC formation climatology suggest that TC formation is preferred in regions of large-scale enhanced low-level convergence. In particular, TC formation is often associated with enhanced convergence zones associated with equatorial Rossby waves (Molinari et al. 2007), the Madden–Julian oscillation (Maloney and Hartmann 2001; Molinari and Vollaro 2000), and the monsoon trough (Briegel and Frank 1997). Based on these findings, the 850-hPa horizontal divergence was included as a parameter. The 850-hPa divergence (HDIV) for each subregion in the algorithm domain is calculated from the GFS wind fields:

$$\text{HDIV} = \frac{\overline{du}}{dy} + \frac{\overline{dv}}{dx},$$

where $\overline{du/dy}$ and $\overline{dv/dy}$ are the values du/dy and dv/dy, respectively, averaged over a 12° × 12° subgrid of the GFS data field that is centered on the algorithm subregion.

i. Cloud-cleared water vapor brightness temperature

Midlevel moisture levels may influence the development of tropical cyclones by modulating convective activity. Dry air at middle levels can have a negative impact on convective activity by reducing the updraft buoyancy via entrainment and decreasing the precipitation efficiency within developing systems (Ruprecht and Gray 1974; Gray 1975; Bister and Emanuel 1997). As described by Moody et al. (1999), the geostationary satellite water vapor imagery in cloud-free regions is sensitive to the relative humidity in the mid- to upper troposphere. Hence, the average brightness temperature (BTWARM) within each 5° × 5° latitude–longitude subregion is calculated after removing all pixels colder than −40°C and is used as an approximation of the midlevel moisture.

j. Percent cold pixel coverage

Observational studies have found that deep convective bursts are often a precursor to TC formation (Gentry et al. 1970; McBride and Zehr 1981; Zehr 1992; Molinari

et al. 2004). To include this environmental signature in our algorithm, a parameter to quantify deep convective activity was developed. This parameter (PCCOLD) uses water vapor (6.7 μm) brightness temperatures and determines the percent of pixels within each 5° × 5° latitude–longitude subregion that is colder than −40°C.

k. Climatological 24-h TC formation probability

Monthly climatological TC formation probabilities were calculated by adding up the total number of TC formations in each 5° × 5° latitude–longitude subregion for each month over the 1949–2005 best-track dataset and then dividing by the number of years (57). These monthly values were then divided by the total number of days in each month to obtain an average daily climatological TC formation probability for each month. Finally, the 24-h climatological probability parameter (CPROB) was calculated by linearly interpolating between these average daily probabilities.

REFERENCES

Beven, J. L., 1999: The boguscane–A serious problem with the NCEP Medium-Range Forecast model in the Tropics. Preprints, *23rd Conf. on Hurricanes and Tropical Meteorology*, Dallas, TX, Amer. Meteor. Soc., 845–848.

Bister, M., and K. A. Emanuel, 1997: The genesis of Hurricane Guillermo: TEXMEX analyses and a modeling study. *Mon. Wea. Rev.,* **125,** 2662–2682.

Bracken, W. E., and L. F. Bosart, 2000: The role of synoptic-scale flow during tropical cyclogenesis over the North Atlantic Ocean. *Mon. Wea. Rev.,* **128,** 353–376.

Briegel, L. M., and W. M. Frank, 1997: Large-scale forcing of tropical cyclogenesis in the western North Pacific. *Mon. Wea. Rev.,* **125,** 1397–1413.

Davis, C., C. Snyder, and A. C. Didlake Jr., 2008: A vortex-based perspective of eastern Pacific tropical cyclone formation. *Mon. Wea. Rev.,* **136,** 2461–2477.

DeMaria, J., A. Knaff, and B. H. Connell, 2001: A tropical cyclone genesis parameter for the tropical Atlantic. *Wea. Forecasting,* **16,** 219–233.

DeMaria, M., M. Mainelli, L. K. Shay, J. A. Knaff, and J. Kaplan, 2005: Further improvements in the Statistical Hurricane Intensity Prediction Scheme (SHIPS). *Wea. Forecasting,* **20,** 531–543.

Elsberry, R. L., W. M. Frank, G. J. Holland, J. D. Jarrell, and R. L. Southern, 1987: *A Global View of Tropical Cyclones*. University of Chicago Press, 185 pp.

Emanuel, K. A., and D. S. Nolan, 2004: Tropical cyclone activity and global climate. Preprints, *26th Conf. on Hurricanes and Tropical Meteorology*, Miami, FL, Amer. Meteor. Soc., 240–241.

Frank, N. L., and G. Clark, 1980: Atlantic tropical systems of 1979. *Mon. Wea. Rev.,* **108,** 966–972.

Frank, W. M., and P. E. Roundy, 2006: The role of tropical waves in tropical cyclogenesis. *Mon. Wea. Rev.,* **134,** 2397–2417.

Gentry, R. C., T. T. Fujita, and R. C. Sheets, 1970: Aircraft, spacecraft, satellite and radar observations of Hurricane Gladys, 1968. *J. Appl. Meteor.,* **9,** 837–850.

Gray, W. M., 1968: Global view of the origin of tropical disturbances and storms. *Mon. Wea. Rev.,* **96,** 669–700.

——, 1975: Tropical cyclone genesis in the western North Pacific. Tech. Paper 16-75, Dept. of Atmospheric Sciences, Colorado State University, 66 pp. [Available from Dept. of Atmospheric Sciences, Colorado State University, Fort Collins, CO 80523.]

——, 1979: Hurricanes: Their formation, structure and likely role in the tropical circulation. *Meteorology over the Tropical Oceans,* D. B. Shaw, Ed., Royal Meteorological Society, 155–218.

——, 1984: Atlantic seasonal hurricane frequency. Part I: El Niño and 30 mb quasi-biennial oscillation influences. *Mon. Wea. Rev.,* **112,** 1649–1668.

Harr, P. A., cited 2007: Joint hurricane testbed: Final report—Objective and automated assessment of operational global forecast predictions of tropical cyclone formation and life cycle. [Available online at http://www.nhc.noaa.gov/jht/final_rep/ENharr_JHTfinalreport_03-05.pdf.]

Hendricks, E. A., and M. T. Montgomery, 2006: Rapid scan views of convectively generated mesovortices in sheared Tropical Cyclone Gustav (2002). *Wea. Forecasting,* **21,** 1041–1050.

——, ——, and C. A. Davis, 2004: The role of ''vortical'' hot towers in the formation of Tropical Cyclone Diana (1984). *J. Atmos. Sci.,* **61,** 1209–1232.

Hennon, C. C., and J. S. Hobgood, 2003: Forecasting tropical cyclogenesis over the Atlantic basin using large-scale data. *Mon. Wea. Rev.,* **131,** 2927–2940.

Kalnay, E., and Coauthors, 1996: The NCEP/NCAR 40-Year Reanalysis Project. *Bull. Amer. Meteor. Soc.,* **77,** 437–471.

Knaff, J. A., T. A. Cram, A. B. Schumacher, J. P. Kossin, and M. DeMaria, 2008: Objective identification of annular hurricanes. *Wea. Forecasting,* **23,** 17–28.

Leipper, D. F., 1967: Observed ocean conditions and Hurricane Hilda, 1964. *J. Atmos. Sci.,* **24,** 182–186.

Levitus, S., 1982: *Climatological Atlas of the World Ocean.* NOAA Prof. Paper 13, 173 pp.

Malkus, J. S., and H. Riehl, 1960: On the dynamics and energy transformation in steady-state hurricanes. *Tellus,* **12,** 1–20.

Maloney, E. D., and D. L. Hartmann, 2001: The Madden–Julian oscillation, barotropic dynamics, and North Pacific tropical cyclone formation. Part I: Observations. *J. Atmos. Sci.,* **58,** 2545–2558.

Mason, S. J., and N. E. Graham, 1999: Conditional probabilities, relative operating characteristics, and relative operating levels. *Wea. Forecasting,* **14,** 713–725.

McBride, J. L., 1995: Tropical cyclone formation. *Global Perspectives on Tropical Cyclones*, R. L. Elsberry, Ed., WMO/TD 693, Rep. TCP-38, World Meteorological Organization, 63–105.

——, and R. M. Zehr, 1981: Observational analysis of tropical cyclone formation. Part II: Comparison of non-developing versus developing systems. *J. Atmos. Sci.,* **38,** 1132–1151.

Molinari, J., and D. Vollaro, 2000: Planetary- and synoptic-scale influences on eastern Pacific tropical cyclogenesis. *Mon. Wea. Rev.,* **128,** 3296–3307.

——, ——, S. Skubis, and M. Dickinson, 2000: Origins and mechanisms of eastern Pacific tropical cyclogenesis: A case study. *Mon. Wea. Rev.,* **128,** 125–139.

——, ——, and K. L. Corbosiero, 2004: Tropical cyclone formation in a sheared environment: A case study. *J. Atmos. Sci.,* **61,** 2493–2509.

——, K. Lombardo, and D. Vollaro, 2007: Tropical cyclogenesis within an equatorial Rossby wave packet. *J. Atmos. Sci.,* **64,** 1301–1317.

Montgomery, M. T., M. E. Nicholls, T. A. Cram, and A. B. Saunders, 2006: A vortical hot tower route to tropical cyclogenesis. *J. Atmos. Sci.,* **63,** 355–386.

Moody, J. L., A. J. Wimmers, and J. C. Davenport, 1999: Remotely sensed specific humidity: Development of a derived product from the GOES Imager channel 3. *Geophys. Res. Lett.,* **26,** 59–62.

Murphy, A. H., 1973: A new vector partition of the probability score. *J. Appl. Meteor.,* **12,** 595–600.

Ooyama, K. V., 1990: A thermodynamic foundation for modeling the moist atmosphere. *J. Atmos. Sci.,* **47,** 2580–2593.

Palmén, E. H., 1948: On the formation and structure of tropical cyclones. *Geophysics,* **3,** 26–38.

Pasch, R. J., P. A. Harr, L. A. Avila, J.-G. Jiing, and G. Eliott, 2006: An evaluation and comparison of predictions of tropical cyclone cyclogenesis by three global forecast models. Preprints, *27th Conf. on Hurricanes and Tropical Meteorology,* Monterey, CA, Amer. Meteor. Soc., 14B.5. [Available online at http://ams.confex.com/ams/pdfpapers/108725.pdf.]

Perrone, T. J., and P. R. Lowe, 1986: A statistically derived prediction procedure for tropical storm formation. *Mon. Wea. Rev.,* **114,** 165–177.

Riehl, H., 1948: On the formation of typhoons. *J. Meteor.,* **5,** 247–264.

Ruprecht, E., and W. M. Gray, 1974: Analysis of satellite-observed tropical cloud clusters. Tech. Paper 219, Dept. of Atmospheric Sciences, Colorado State University, 91 pp. [Available from Dept. of Atmospheric Sciences, Colorado State University, Fort Collins, CO 80523.]

Sampson, C. R., and A. J. Schrader, 2000: The Automated Tropical Cyclone Forecasting System (version 3.2). *Bull. Amer. Meteor. Soc.,* **81,** 1231–1240.

Shapiro, L. J., and S. B. Goldenberg, 1998: Atlantic sea surface temperatures and tropical cyclone formation. *J. Climate,* **11,** 578–590.

Simpson, J., J. B. Halverson, B. S. Ferrier, W. A. Petersen, R. H. Simpson, R. Blakeslee, and S. L. Durden, 1998: On the role of ''hot towers'' in tropical cyclone formation. *Meteor. Atmos. Phys.,* **67,** 15–35.

Stephenson, D., 2004: Skill measures for forecasts of extreme rare events. *Abstracts, Climate Extremes and Risk Reduction Conference*, London, United Kingdom, Lighthill Institute of Mathematical Science, London, England. [Available online at http://www.ucl.ac.uk/lims/events/LIMSConf30Nov04.htm.]

Wilks, D. S., 2006: *Statistical Methods in the Atmospheric Sciences*. 2nd ed. Academic Press, 467 pp.

Zehr, R. M., 1992: Tropical cyclogenesis in the western north Pacific. NOAA Tech. Rep. NESDIS 61, 181 pp. [Available from NOAA/National Environmental Satellite, Data, and Information Service, Washington, DC 20233.]